ehydes and other oxo compounds via catalytic hydroformylation of olefins is one of the industrially important homogeneous reactions. Catalytic hydroformylation of alkenes for the production of approximately 8.6 million tons/year of aldehydes for use in the manufacture of soaps, detergents and plastisizers [1-2] is commercially done. However, in some cases, the deviations from the desired product due to the formation of various intermediate species may occur, mainly because of complicated reaction cycle involved in the hydroformylation reactions. For example, it has been reported [3] that with the $Co_2(CO)_8$ as a catalyst, the formation of alcohol occurs after the formation of aldehyde and in this case $HCo(CO)_3$ acts as a the reducing agent. During hydroformylation, various other side-reactions, *viz*., Aldol reaction, acetal formation, Tishchenko reaction, isomerization, polymerization and hydrogenation [4] may also take place, depending on the reaction conditions and nature of the catalysts used.

As for the central metal is concerned for hydroformylation catalysts studies, rhodium and cobalt metals are the widely studied active metals. However, the studies explain exact reasons for the low activity of other platinum group metals/metal complexes. Ruthenium, as a hydroformylation catalyst has shown significantly lower activities than those for rhodium and cobalt metals. The monomeric ruthenium-carbonyl-triphenylphosphine species yields [5] only modest normal to branched regioselectivity under relatively severe conditions. For example, after 22 h at 120^0C, 100 bar pressure, $Ru(CO)_2(PPh_3)_2$ gives only 86% conversion and 2.4:1.0 linear/branched aldehyde isomer ratio. However, excess PPh_3, improves the selectivity to linear/branched ratio but at the expense of dramatic decrease in the rate of reaction. In another example, cluster catalyst $[HRu_3(CO)_{11}]^{-1}$ shows good catalytic activity and high regioselectivity using propylene as a substrate [6-8]. In monoglyme as a solvent, at 80^0C and partial pressure for C_3H_6, CO, H_2 of 0.34, 0.22 and 0.11 bar respectively, the catalyst turnover number is reported to be 34.3 with 49.4:1.0 linear/branched ratio of the aldehyde.

We have been exploring the possibility of such non-rhodium based complexes, which are well known for other homogeneous reactions, to understand the basic reason of their low activity for the hydroformylation reactions. For that purpose, we have chosen

)ruthenium(II), $RuCl_2(PPh_3)_3$ **1**, which is well known ogenation of olefinic double bond. In our investigations on $RuCl_2(PPh_3)_3$, **1** catalyzed hydroformylation of propylene, low activity of this complex was observed towards hydroformylation reaction under mild pressure conditions.

In addition to that, the studies on solution chemistry involving, kinetic, mechanistic, equilibrium and thermodynamic investigations on the *in-situ* formed carbonyl complexes of ruthenium are fundamentally important to understand the nature of interaction of carbon monoxide with ruthenium complexes, which is one of the key intermediate steps involved during the catalytic cycle of hydroformylation reaction. Kinetic, mechanistic, equilibrium and thermodynamic studies, on one side provide, significant basic and applied inputs for optimizing a reaction to develop for large scale chemicals production, on other side these studies potentially provide valuable information also, to understand the limitations of the reactions, which are important to overcome for incremental improvement and up-gradation of a process. Furthermore, most of the carbonylation and hydroformylation reactions catalyzed by metal complexes are studied in non-aqueous medium and very less attention is paid towards the studies in aqueous medium [9-13].

This chapter deals with the investigations, on understanding the solution chemistry of interaction of carbon monoxide with dichlorotris(triphenylphosphine)ruthenium(II), $RuCl_2(PPh_3)_3$, **1** and its application as homogeneous catalyst for hydroformylation of propylene. Kinetic, equilibrium and thermodynamic studies were performed on the formation of carbonyl complex by the interaction of *in-situ* formed dichlorobis(triphenylphosphine)(solvent)ruthenium(II), $RuCl_2(PPh_3)_2(S)$, **1a** and carbon monoxide in a 1:1 mixed aqueous solvent, in a 50% (v/v) mixture of water and 1,4 dioxan in the temperature range 10-40^{0}C at atmospheric pressure of CO. The hydroformylation of propylene using $RuCl_2(PPh_3)_3$, **1** as a catalyst was carried out 9 bar pressure and 175^{0}C temperature in ethanol as a solvent. Under the employed reaction conditions lower conversion and selectivities were observed with $RuCl_2(PPh_3)_3$, **1** catalyst. The separation of crystalline solid was observed during hydroformylation reaction in the autoclave reactor. The detail investigation of formation of the crystalline solids were done and the observed lower conversion towards hydroformylation products in ethanol as a solvent with complex **1** was explained in terms of formation of inactive species.

Propylene (99.5%) and syn-gas (99.8%) were purchased from Alchemie Gases & Chemicals Pvt. Ltd. Mumbai, India. Ruthenium salt, $RuCl_3.3H_2O$, was purchased from Johnson Mathew (U.K.). Triphenylphosphine was purchased from E. Merck, India. The organic solvents 1, 4 dioxan, ethanol and methanol were purchased from Rankem, India and purified using reported methods [14]. The solvents 1,4 dioxan and water were always used after double distillation for all solution studies. For the kinetic studies, carbon monoxide was prepared [15] by the reaction of sodium formate and sulfuric acid, and purified through a tower of KOH pellets. Argon gas was used to maintain inert atmosphere in the reaction mixtures in solution since ruthenium complexes are highly oxygen sensitive.

2.2.2. Synthesis and characterization of the $RuCl_2(PPh_3)_3$ complex

The complex $RuCl_2(PPh_3)_3$ was prepared by reported procedure [16] with 75% yield. FT-NMR (^1H, ^{31}P) and FT-IR spectroscopy for the characterization of metal complex $RuCl_2(PPh_3)_3$ was done by using Bruker Avance DPX 200MHz FT-NMR and Perkin Elmer Spectrum GX FT-IR systems, respectively. C, H and N elemental analyses were done on Perkin Elmer CHNS/O 2400 analyzer.

The ^{31}P-NMR spectrum of the complex $RuCl_2(PPh_3)_3$ (in CH_2Cl_2) at 43.04 ppm which verified the formation of the complexes. In the FT-IR, the appearance of ɜ (Ru-P) band at 517 cm^{-1} confirmed the formation of corresponding ruthenium complexes. The C (%), H (%) was observed to be; calculated (found): C: 67.7 (67.5); H: 4.7 (4.5).

2.2.3. Physical studies

UV-VIS spectra were recorded on Shimadzu UV-160 spectrophotometer equipped with TCC-240A temperature controller. Matched 10 or 5 mm cells were used to record the spectra for kinetic and equilibrium studies. The electrochemical studies were conducted on C.H. Instruments, Electrochemical Workstation using glassy carbon as working electrode, Pt as auxiliary and Ag/AgCl as reference electrodes.

2.2.4. Equilibrium constants and CO solubility measurements

The equilibrium constants, corresponding to dissociation of one of the coordinated triphenylphosphine [17] from original complex, $RuCl_2(PPh_3)_3$, **1**, to form

osphine)ruthenium(II), $RuCl_2(PPh_3)_2(S)$, **1a** and the uthenium carbonyl complex $RuCl_2(CO)(PPh_3)_2$, **2**, were determined spectrophotometrically in a 1:1 (v/v) mixture of water-dioxan solvent.

$$\underset{\mathbf{1}}{RuCl_2(PPh_3)_3} \overset{K}{\rightleftharpoons} \underset{\mathbf{1a}}{RuCl_2(PPh_3)_2(S)} + PPh_3$$

$$\underset{\mathbf{1a}}{RuCl_2(PPh_3)_2(S)} + CO \xrightarrow{k} \underset{\mathbf{2}}{RuCl_2(CO)(PPh_3)_2}$$

The solubility of CO in 1:1 (v/v) mixture of water-dioxan was obtained manometrically [19] at 1 bar pressure. The absorption of CO was measured by using a glass manometric apparatus provided by the leak-proof Springham stopcocks. High-vacuum silicon grease was applied to stopcocks to keep the system airtight. The temperature of constantly stirred 1:1 (v/v) mixture of water-dioxan solvent (50 ml) was maintained through a jacketed glass cell by circulating water from a thermostat kept at a desired temperature (±0.1 K). The system was evacuated and flushed at 1 bar with CO several times to ensure that a complete CO atmosphere prevails in the solvent. In order to minimize the effect of solvent vapor, a blank was run simultaneously under the same conditions of temperature, pressure and volume. The maximum absorption of CO was measured manometrically by noting the change in the levels of the indicator solution in the measuring burette.

2.2.5. Kinetic measurements

The kinetics of complexation of carbon monoxide with $RuCl_2(PPh_3)_2(S)$, **1a**, was measured spectrophotometrically by monitoring the absorption maximum of carbonyl complex **2** at 430 nm. The wavelength of maximum absorbance (λ_{max}) for the carbonyl complex **2** was determined by mixing saturated CO solution in $RuCl_2(PPh_3)_3$ complex in argon atmosphere and recording the spectra. Kinetic data were computed from the slopes of the first order kinetic plots of log $(A_\infty-A_0)/(A_\infty-A_t)$ versus time where A_0, A_t and A_∞ are the absorbance at zero, experimental and infinite times respectively. A freshly prepared saturated solution of CO in 1:1(v/v) mixture of doubly distilled water and 1, 4 dioxan was used in all the kinetic runs. The concentration of CO in the experiments was varied by diluting the saturated solution to the desired concentrations. The reactants were

ature for 40 minutes in argon atmosphere before mixing. was always maintained in the reactions and total volume (50 ml) of the reaction mixture was kept constant.

2.2.6. Thermodynamic measurements

Formation constants (K_1) for the *in-situ* formed Ru^{II}-carbonyl complex **2**, in 1:1 (v/v) mixture of water-dioxan were determined spectrophotometrically by reported method [20] at different temperatures. Rate constants for formation of carbonyl complex **2** were also computed at different temperatures. Arrhenius equation, Eyring equation and vanô Hoff equation were used to determine the thermodynamic quantities associated with formation of complex **2**, by interaction of carbon monoxide with *in-situ* formed complex **1a.**

The thermodynamic parameters [21] corresponding to complex **2**, formation constant, K_1, were computed using Equations (2.1)-(2.3). The enthalpy (ΔH^0) was obtained from the slope of the plot of log (K_1) v/s 1/T.

$$\Delta H^0 = -2.303R \text{ (Slope)} \quad (2.1)$$

$$\Delta G^0 = -2.303RT \log K_1 \quad (2.2)$$

$$\Delta S^0 = (\Delta H^0 - \Delta G^0)/T \quad (2.3)$$

The activation parameters corresponding to rate constant were computed using Equations (2.4)-(2.6). Activation energy E_a was obtained from the slopes of log (k) v/s 1/T.

$$E_a = -2.303R \text{ (Slope)} \quad (2.4)$$

$$\Delta H^{\#} = E_a \text{ ï } RT \quad (2.5)$$

$$\Delta S^{\#} = 2.303R \log (hkN/RT) + \Delta H^{\#}/T \quad (2.6)$$

Where, R = gas constant, h = Planck constant, N = Avogadro number, T = Temperature in Kelvin, K_1 = formation constant and k = rate constant

2.2.7. Hydroformylation reaction

2.2.7.1. The autoclave reactor

All hydroformylation experiments were carried out in 100 ml stainless steel autoclave reactor (Autoclave Engineers, U.S.A.) equipped with a controlling unit. The reactor was kept in a fume cupboard equipped with a strong exhaust fan. The autoclave

ng up to 350 bar pressure and 400^{0}C temperature with a ave was designed with three-gas liner one for gas inlet, second for gas ventilation and third as a sampling valve. The autoclave was provided with propeller type stirrer. A pressure transducer monitor system with high precision (± 2%) was also connected to the reactor for online measurement of pressure drop in the autoclave during the course of reaction. The temperature (±0.5^{0}C) and speed of stirrer (±20 rpm) can be controlled by the controlling unit, which is attached with the autoclave reactor. The controlling unit displays digitally the rpm value of stirrer, the pressure inside the reactor (in psi) and the temperatures (in ^{0}C) inside and outside the autoclave reactor. The propellers in the reactor were fixed at a position in which an improved gas distribution was observed leading to intensive gas-liquid contacts with gas bubbles reacting to all parts of the liquid. The spraying of gases supplied inside the reactor occurred in such a way that sprayed gases cover all parts of the reactor.

The safety aspects were always taken into sincere considerations while dealing with carbon monoxide related high-pressure reactions. All the high-pressure reactions were done in a high-pressure laboratory, which was specially made for conducting experiments at high pressure and temperature. A carbon monoxide gas detector system equipped with alarm, sensing for human tolerance limit (50 part per million) of CO, is kept in laboratory to avoid CO inhaling, in case of any leakage during handling of CO and its reaction. In addition to that, there is always a medical grade oxygen gas kept in laboratory to inhale in case of any emergency. The schematic representation of the autoclave reactor used for hydroformylation reactions is shown below in Figure 2.1.

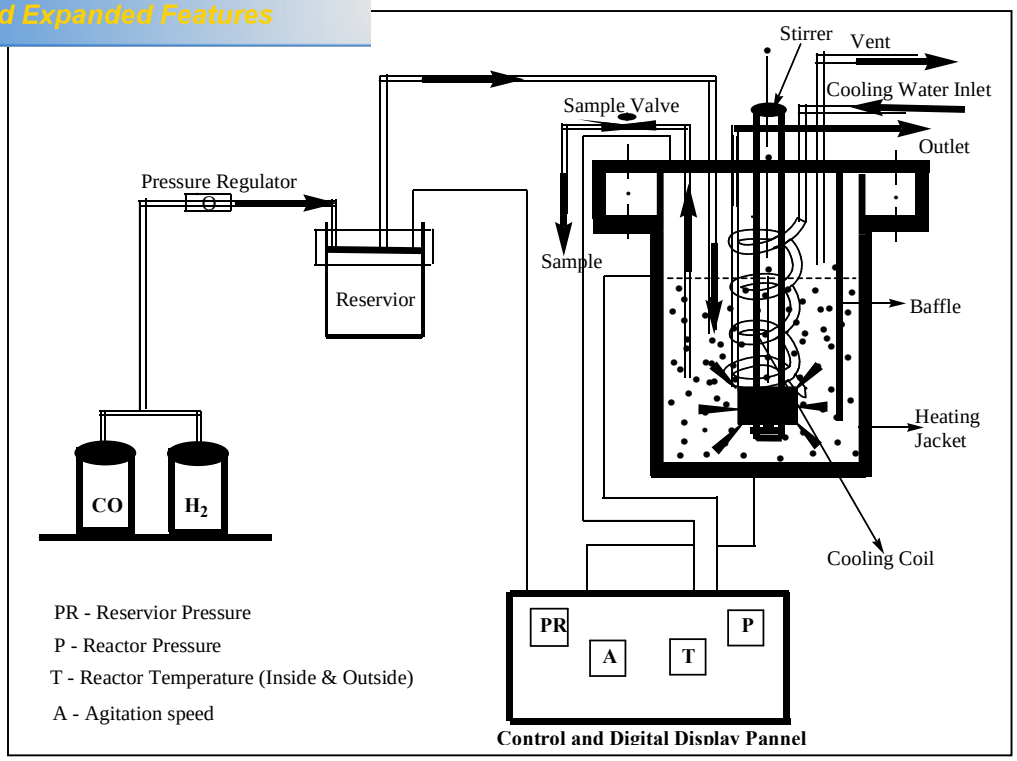

Figure 2.1. The schematic diagram of the autoclave reactor

2.2.7.2. The hydroformylation reactions

In a typical hydroformylation experiment, the desired quantity of $RuCl_2(PPh_3)_3$, **1**, catalyst dissolved in ethanol (50 ml) was charged in the autoclave. The autoclave was twice flushed with nitrogen prior to successively introducing propylene at desired pressure. The reactor was then brought to desired reaction temperature. After the set reaction temperature, the syn-gas was supplied to the reactor up to desired pressure. The hydroformylation reaction was initiated by starting the magnetic stirrer upto desired rpm. The reaction was then continued at constant pressure, by supply of carbon monoxide and hydrogen (1:1) from reservoir vessel. Whenever the supply of carbon monoxide and hydrogen was from separate cylinders instead of reservoir, the carbon monoxide was introduced into the catalyst solution before addition of H_2 to avoid hydrogenation and isomerization as side reactions. After the set reaction time, the autoclave was cooled to room temperature and pressure drops were also noted. The reaction was then quenched by disconnecting the gas supply to the autoclave reactor. It was observed that during the

…action, small amount of solid crystalline materials were …e reaction mixture, which were collected carefully by filtration/decantation.

2.2.7.3. Hydroformylation product analysis

The reaction product analysis was carried out using gas chromatography (GC) (Shimadzu 17A, Japan); the instrument has a 5% diphenyl and 95% dimethyl siloxane universal capillary column (60m length and 0.32mm diameter) and a flame ionization detector (FID). The initial column temperature was increased from 40 to 200^0C at the rate of 10^0C/min. Nitrogen gas was used as the carrier gas. The temperatures of the injection port and FID were kept constant at 200^0C during product analysis. The retention times for different compounds were determined by injecting pure compounds under identical gas chromatography conditions.

2.2.8. Single crystal X-ray analysis

Cell parameters and diffracted intensities for the compound were measured at room temperature on an Enraf-Nonius CAD-4 X-ray diffractometer using graphite monochromatized MoK_α radiation (0.7107Å) in the range $\theta = 2\text{-}25^0$. 25 reflections with θ in the range $7\text{-}10^0$ were used for getting the accurate cell dimensions. Three standard reflections were monitored after every 100 reflections during the entire period of data collection, which showed no significant variation, indicating the stability of the crystal. The crystal orientation, refinement of the cell parameters and intensity measurements were carried out using the program CAD-4 PC [22]. The raw intensity data were corrected for Lorentz polarization effects but not for absorption. The Lorentz polarization corrections and data reduction were carried out using NRCVAX [23] program. The structure was solved by heavy atom method using the program SHELEXL-97 [24]. The full matrix least squares refinement of all non-hydrogen atoms with isotropic temperature factors was carried out until the convergence. After the complete convergence of non-hydrogen atoms anisotropically, the H-atoms were either fixed stereochemically by riding model using SHELEXL-97 or located from the difference Fourier map. The final cycles of least squares refinements, yielded the R-value R_1= 0.0512 (wR_2= 0.1380) for the complex.

and equilibria studies

Studies on characterization of species **1**, **1a** and *in-situ* formed ruthenium carbonyl complex **2** were performed spectrophotometrically by conducting a series of experiments. The *in-situ* formation of mono carbonyl complex **2** was also characterized by electrochemical and FT-IR spectroscopic techniques. $RuCl_2(PPh_3)_3$ was dissolved in 1:1 (v/v) water-dioxan solvent and the recorded time scan solution spectra are given in Figure 2.2. The spectra displayed absorption maxima at 530 nm and a broad band at 795 nm. Similar spectral behavior of **1** displaying absorption maxima at 480 nm and broad band at 750 nm is reported [17] in benzene solvent.

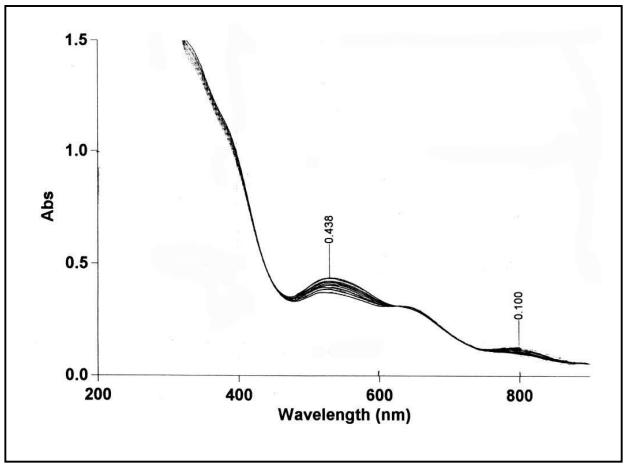

Figure 2.2. Time scan, absorption increasing spectral changes at [**1**] = $5.0x10^{-4}$ M, μ = $5.0x10^{-3}$ M and T= 30^0C without added PPh_3. Initial spectrum is the lowest one at zero time, and the successive spectra were recorded at intervals of 2 min.

In the next experiment, PPh_3 was added in solution of complex **1** at conditions identical to the mentioned above in Figure 2.2. in addition, the time scan spectra were recorded and are shown in Figure 2.3. Addition of excess PPh_3 in complex **1** resulted to give maxima at 530 nm and 650 nm (Figure 2.3.) indicating following equilibrium (Reaction 2.7) being shifted to the left.

$$\underset{\mathbf{1}}{RuCl_2(PPh_3)_3} \overset{K}{\rightleftharpoons} \underset{\mathbf{1a}}{RuCl_2(PPh_3)_2(S)} + PPh_3 \qquad (2.7)$$

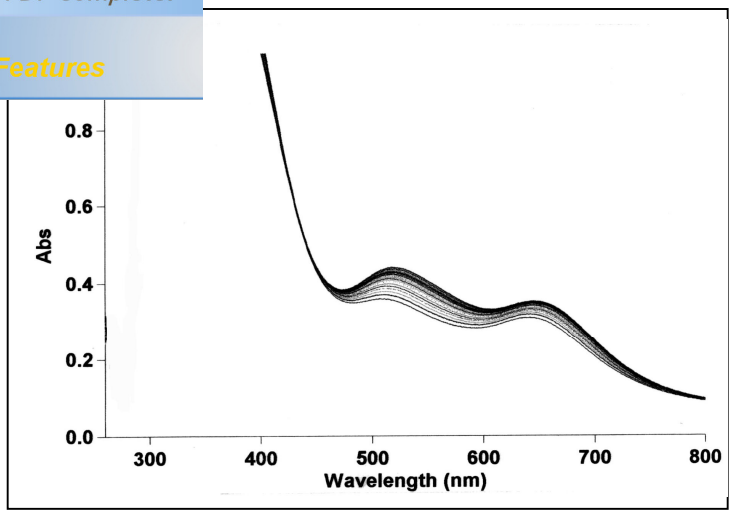

Figure 2.3. Time scan, absorption increasing spectral change at [**1**] = 5.0×10^{-4} M, added [PPh_3] = 2.0×10^{-3} M, μ = 5×10^{-3} M and T= 30^0C. Initial spectrum is the lowest one at zero time, and the successive spectra were recorded at intervals of 1 min.

By adding PPh_3 to complex **1**, maximum absorbance for the complex **1** was observed at the higher phosphine concentration 2×10^{-3} M at 530 nm and 650 nm. The absorbance of a solution containing complex species **1** and **1a** in a 10 mm path length optical cell is given by ε_1[**1**]+ε_{1a}[**1a**], where ε_1 and ε_{1a} are the molar extinction coefficients [17] at the given wavelength. Total concentration of ruthenium $[Ru]_T$ and triphenylphosphine $[(PPh_3)_3]_T$ are given as in Equations (2.8) and (2.9) respectively.

$$[Ru]_T = [\mathbf{1}] + [\mathbf{1a}] \qquad (2.8)$$

$$[PPh_3]_T = [\mathbf{1a}] + [PPh_3]_{added} \qquad (2.9)$$

$$K = [\mathbf{1a}]\,[PPh_3]_T\,[\mathbf{1}]^{-1} \qquad (2.10)$$

The dissociation of PPh_3 from complex **1** {Equation (2.10)} was estimated by reported method [17], by determining the values of ε_1 and ε_{1a}. The value of ε_1 was determined from the limiting spectrum at maximum phosphine concentration from Figure 2.3. An appropriate value of ε_{1a} was estimated from spectra (Figure 2.2.) for the equilibrated solution of **1**, without added PPh_3 by assuming that **1** is completely dissociated at the ruthenium concentration used. Using ε_1 and the approximate ε_{1a} values, dissociation constant K was estimated from the spectra of a set of intermediate added phosphine concentrations in the range from 0.5×10^{-3} to 2.0×10^{-3} M. Using the mean of these K values, the concentrations of **1** and **1a** were then calculated for the solution having spectrum of equilibrated solution of **1** (Figure 2.3.), for allowing a more accurate

omputation of K values. This successive approximation
nt molar extinction coefficient ($M^{-1}cm^{-1}$) for the two wavelengths corresponding to the absorption maxima of $RuCl_2(PPh_3)_3$:ε_1 880 (530 nm), 200 (795 nm) and ε_{1a} 680 (530 nm), 0 (795 nm). The value of dissociation constant K was estimated to be $2.50x10^{-3}$ M at 30^0C. The value of dissociation constant of complex **1** in benzene is reported [17] to be $2.70x10^{-3}$ M at 25^0C in which $1x10^{-3}$ M benzene solution of **1** is found to be about 80% dissociated. Hence, reasonably 80% dissociation of **1** to **1a** was considered for evaluating the *in-situ* concentration of **1a** during the studies.

Complexation of carbon monoxide to form *in-situ* complex **2** by interacting with equilibrated solution of complex **1** was studied by adding CO solution at required experimental conditions at atmospheric pressure. An appropriate quantity of complex **1** dissolved and sufficiently equilibrated (40 minutes) with nitrogen (inert gas) passed in 1:1 (v/v) water-dioxan solvent, containing suitable amount of KCl as electrolyte (solution A) and solution containing dissolved CO (solution B) were made in separate containers and both solutions were kept in a thermostatic bath at the desired temperatures. Hence, complex **1** was sufficiently allowed to dissociate to **1a** to reach the equilibrium before adding CO solution. On mixing solution (A) and solution (B) and subjecting it for spectrophotometric studies revealed that a broad new peak having absorption maxima (λ_{max}) at 430 nm, was formed. An increase in the absorbance with single progress curve (Figure 2.4.) was observed indicating the formation of ruthenium carbonyl complex **2** [25-27]. The formation of ruthenium carbonyl complex **2** was also confirmed by FT-IR of the complexes **1** and **2**. IR spectra of solid sample of complex **1** (KBr pellets) and liquid sample of carbonylated complex **2**, in mixed aqueous solvent, 1:1 (v/v) water-dioxan were recorded and is shown in Figure 2.5. A comparison of IR spectra of complex **1** and **2** clearly showed the formation of a new sharp peak at ν(CO) = 2000 cm^{-1}, characteristic for CO band [27], which is absent in complex **1**.

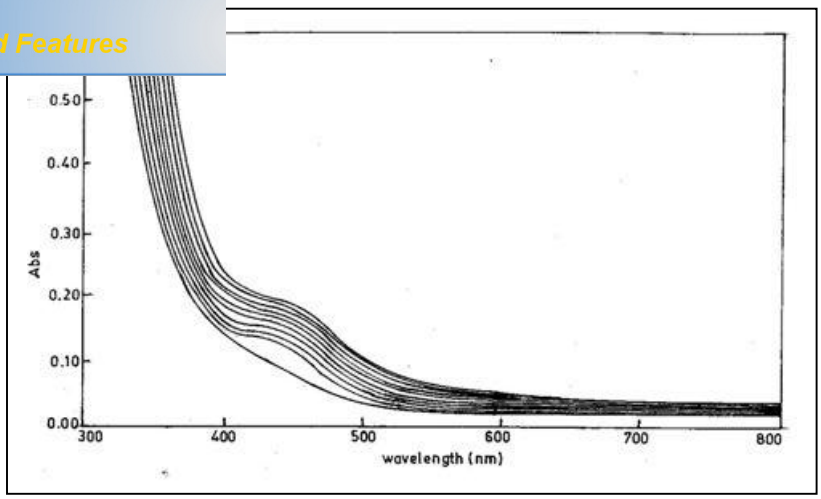

Figure 2.4. Time scan, absorption increasing spectral changes at λ_{max} 430 nm, at interval of 1 min for the formation of complex **2** at [**1**] = $5.0x10^{-4}$ M, [CO] = $2.3x10^{-3}$ M, μ = $5.0x10^{-3}$ M and T= 30^0C. The spectrum of complex **1** in absence of CO, in the identical conditions is the lowest one.

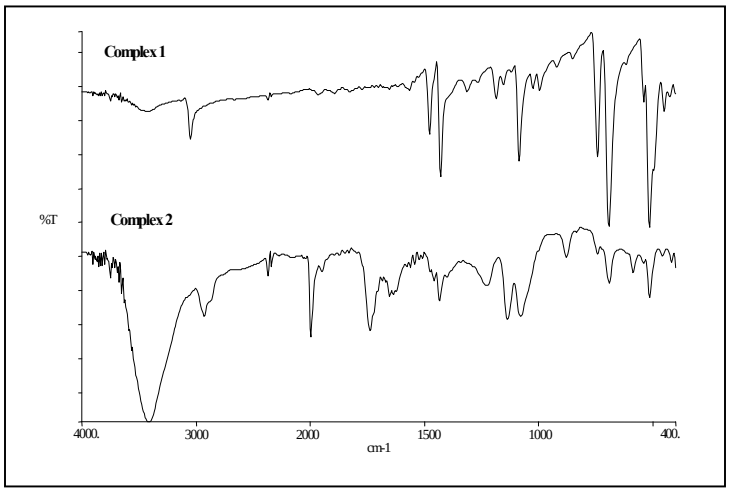

Figure 2.5. FT-IR spectra of (a) complex **1** (KBr pellets) and (b) carbonylated complex **2** (recorded in mixed aqueous solvent 1:1 (v/v) water-dioxan).

The formation of complex **2** was also supported by electrochemical experiments carried out to study the interaction of CO and the oxidation state of ruthenium in the carbonyl complex **2**. Their cyclic voltammogram (CV) are shown in Figure 2.6. The CV of complex **1** exhibited a reversible peak at 0.81 V in the presence of nitrogen corresponding Ru^{II}/Ru^{III} couple. In the presence of CO, under similar conditions, an entirely different CV was obtained. The peak at 0.81 V disappeared and an ill-defined peak, found to be immersed with residual current, appeared in the potential range 1.40 to

ackward reduction gave a peak at 0.60 V in the reverse presence of CO is attributed to the interaction of CO with complex **1** to form complex **2**, in which the ill defined peak undergoing oxidation (Ru^{II}/Ru^{III}), appeared in the higher potential range 1.40 to 1.50 V, shifts from 0.81 V to 1.4-1.50 V at a difference of ~0.65 V. In reverse direction, the peak at 0.60 V corresponds to redox couple Ru^{II}/Ru^{III}.

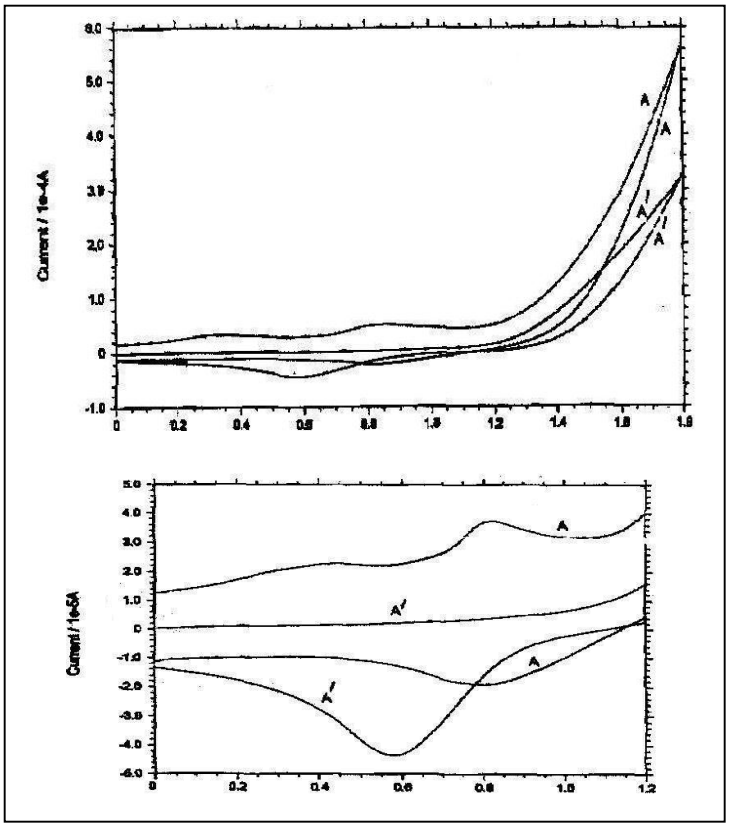

Figure 2.6. Cyclic voltammogramms of complex **1** in the presence of N_2 (A-A) and CO ($A^{/}$-$A^{/}$) at [**1**] = $5.0x10^{-4}$ M, μ = $5.0x10^{-3}$ M and T= 30^0C; (upper Figure) CV shown with residual current and (lower Figure) enlarged portion of the upper CV.

The solubility of CO (Table 2.1.) as expected was found to decrease on increasing the temperature. A comparison of solubility of CO in mixed solvent of 1:1 (v/v) water-dioxan and in water [28] indicated that the solubility in mixed solvent is appreciably higher than that in water. The formation constants K_1 for the complex **2**, given by reaction (2.11) and equation (2.12) were directly calculated by

$$\xrightleftharpoons{K_1} \underset{\mathbf{2}}{RuCl_2(CO)(PPh_3)_2} \qquad (2.11)$$

$$K_1 = \frac{[\mathbf{2}]}{[\mathbf{1a}]\,[CO]} \qquad (2.12)$$

spectrophotometric method [20] at different temperatures and are listed in Table 2.1. The order of the magnitude of these values indicated that the intermediate complex **2** is thermodynamically sufficiently stable to study its kinetics studies spectrophotometrically.

Table 2.1. Formation constant of complex **2** and solubility of CO in 1:1 (v/v) in water-dioxan

Temperature (^{0}C)	Formation constant, K_1 x10^{-4} (M^{-1})	[Solubility of CO] x10^3 (M)	[Solubility of CO] x10^3 (M) (in water)
10	7.40	3.36	1.25
20	3.43	2.73	1.01
30	2.59	2.29	0.85
40	1.75	1.97	0.73

2.3.2. Kinetic studies

The kinetics of complexation of CO with complex **1a** was studied by monitoring the peak at 430 nm for the formation of complex $RuCl_2(CO)(PPh_3)_2$ **2**, as a function of the concentration of complex **1a**, carbon monoxide and electrolyte KCl and the results are listed in Table 2.2. The kinetics of complex **2** formation was found to follow first order dependence in the concentration of complex **1a**. First order kinetic plots of log $(A_\infty-A_0)/(A_\infty-A_t)$ v/s time (Figure 2.7.) were linear. The complexation reactions were studied by conducting the experiments at different concentrations of CO, for which saturated solution of CO was diluted by 1:1 (v/v) waterï dioxan solvent in desired proportions and used to see the effects of variation of CO concentration on the rate of formation of complex **2**, by keeping the concentrations of other reactants and physical conditions constant.

nation of complex **2** at 30^0C

		[KCl]x10^2 (M)	k_{obs}x10^2 (min^{-1})	k ($M^{-1}min^{-1}$)
1	1.00	0.5	21.78	94.70
2	1.00	1.0	22.50	97.82
3	1.00	2.5	21.71	94.40
4	1.00	5.0	21.47	93.35
5	0.33	0.5	7.10	93.54
6	0.50	0.5	11.30	98.26
7	0.50	1.5	11.34	98.60
8	0.75	0.5	17.00	98.55

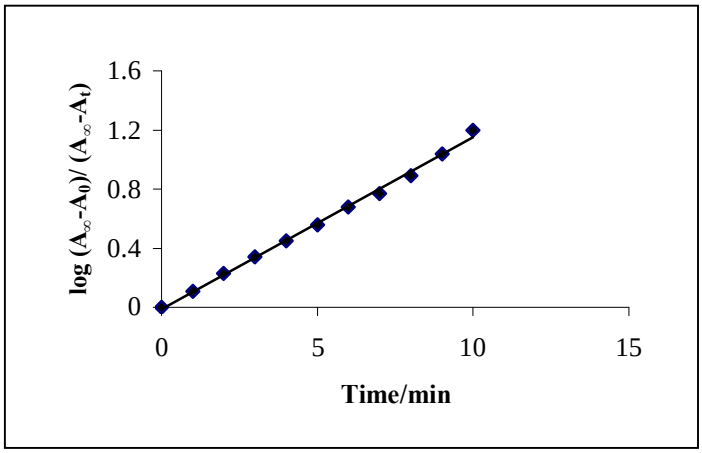

Figure 2.7. First order kinetic plot for the formation of complex **2** at [**1**] = 2.5x10^{-4} M, μ = 5.0x10^{-3} M, [CO] = 2.3x10^{-3} M and T= 30^0C.

A linear increase (Figure 2.8.) in the rate constants k_{obs} with increasing initial concentration of CO indicated first order dependence in CO concentration {d(logk_{obs})/ d(log [CO]) ~1}. In order to study effects of the ionic strength, kinetic experiments performed at suitable low concentrations of KCl in the ionic strength range (0.5-5.0)x10^{-2} M, showed no change in k_{obs} (Table 2.2.). Spectrophotometrically and manometrically determined stoichiometry of the complexation reaction indicated that one equivalent of CO was consumed per equivalent of **1a**.

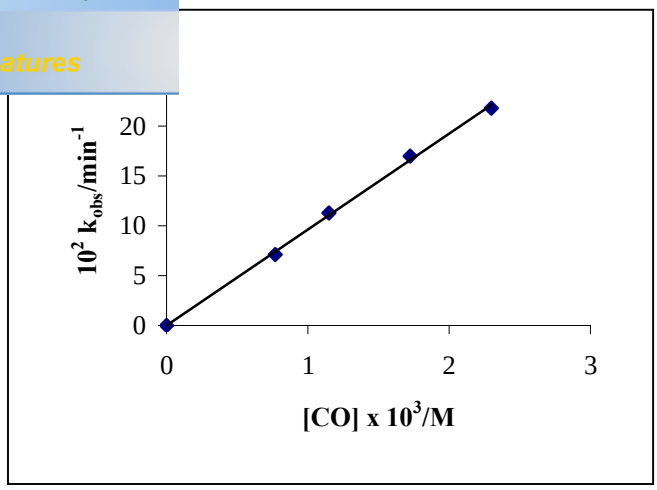

Figure 2.8. Kinetic plot showing the effect of the variation of CO concentration on the rate of formation of complex **2** at [**1**] = 2.5×10^{-4} M, $\mu = 5.0\times10^{-3}$ M and T= 30^0C.

Since both the reactants, complex **1a** and CO are found kinetically equally active showing first order dependence in each, the molar extinction coefficient of complex **2** was determined by measuring the maximum absorbance recorded at 430 nm as a function of the concentration of complex **1a** and CO. In the presence of excess carbon monoxide, assuming all the concentration of complex **1a** is involved in the formation of complex **2**, the molar extinction coefficient at 430 nm (ε^{430}_{max}) determined is 800 $M^{-1}cm^{-1}$.

Kinetic dependence and experimental evidences are explained in terms of equilibrium (2.7) and reaction (2.13) in which complex **1** first dissociates to **1a** by loosing a coordinated PPh_3 molecule in equilibrium step K, followed by complexation of **1a** with CO to form carbonyl complex **2** in step k.

$$\underset{\mathbf{1a}}{RuCl_2(PPh_3)_2(S)} + CO \xrightarrow{k} \underset{\mathbf{2}}{RuCl_2(CO)(PPh_3)_2} \qquad (2.13)$$

Dissociation constant K, 2.50×10^{-3} M at 30^0C and $\mu = 5\times10^{-3}$ M, KCl determined spectrophotometrically [17] {(Equation 2.10)} in 1:1 (v/v) water-dioxan solvent was found to be comparable with the value reported in the solvent benzene.

Extensive dissociation of PPh_3 from complex **1** in millimolar concentrations are well established [17] in two organic solvents benzene and DMF. Variation of KCl concentration having negligible effect on complexation of CO indicated insignificant

e rate expression for the complexation reaction of **1a** with

of k_{obs} is written as:

$$d[\mathbf{2}]/dt = k\,[\mathbf{1a}]\,[CO] \qquad (2.14)$$

$$k_{obs} = (d[\mathbf{2}]/dt)/[\mathbf{1a}] = k\,[CO] \qquad (2.15)$$

The overall second order rate constants k (k_{obs}/[CO]) determined by Equation (2.15) and given in Table 2.2., having an average value, k = 96.40 $M^{-1}min^{-1}$ at 30^0C, found almost constant at a given temperature supported that an overall second order kinetics is involved in this complexation reaction.

The kinetic analysis done as a function of both, the rate {k, Reaction (2.13)} and equilibrium constant {K, reaction (2.7)} gives the rate expression as:

$$d[\mathbf{2}]/dt = k[\mathbf{1a}][CO] = k\,K[\mathbf{1}][CO]/[PPh_3] \qquad (2.16)$$

$$k_{obs} = k\,K[CO]/[PPh_3] \qquad (2.17)$$

Kinetic experiment conducted for carbonylation of **1a** to **2**, with added $2x10^{-3}$ M of PPh_3 in identical conditions of Run 1 (Table 2.2.) giving lower value of k_{obs} ($15.06x10^{-2}$ min^{-1}) indicated that the added PPh_3 contributes towards the inhibition of carbonylation of **1a**, which is in agreement of Equation (2.16) and (2.17). The initial rates of dissociation of PPh_3 (without added PPh_3) from complex **1** to give **1a** ($9.05x10^{-6}$ M min^{-1}) and carbonylation of **1a** to give **2** ($7.5x10^{-6}$ $Mmin^{-1}$) revealed that in present experimental conditions, the dissociation of PPh_3 is reasonably faster than the carbonylation. Additionally, the complex **1** was sufficiently allowed to be equilibrated to dissociate PPh_3 to form **1a**, for each carbonylation experiment, before adding CO at each temperature. Hence in the present experimental conditions the *in-situ* formed **1a** reacted with CO to give complex **2**.

2.3.3. Thermodynamic studies

The rates of formation (k_{obs}) of complex **2** were studied at various temperatures in the range of 10-40^0C in order to see the effects of temperature on the rate of complexation and to evaluate the activation parameters. The temperature-dependence rate constants and activation parameters are given in Table 2.3. and Table 2.4. respectively.

...e on the rate of formation of complex **2**

	(^{0}C)	[CO] x 10^3 (M)	[KCl]x10^2 (M)	k_{obs}x10^2 (min^{-1})
1	10	3.36	0.5	7.62
2	20	2.73	0.5	14.13
3	30	2.29	0.5	24.54
4	40	1.97	0.5	41.68

Table 2.4. Activation and thermodynamic parameters for formation of complex **2**

Activation parameters	Thermodynamic parameter
E_a = 38.4 ± 2.5 kJ mol^{-1}	ΔH^0 = -33.5 ± 4.5kJ mol^{-1}
$\Delta H^{\#}$ = 35.9 ± 2.5 kJ mol^{-1}	ΔS^0 = -25 ± 8 JK^{-1} mol^{-1}
$\Delta S^{\#}$ = -122.0 ± 6.0 $JK^{-1}mol^{-1}$	ΔG^0 = -25.7 ± 2.0 kJ mol^{-1}

Since the solubility of CO also decreases with temperature, the rate of complexation at different temperatures were calculated by taking into account the temperature dependence concentration of CO. The rate of complexation was found to increase (Table 2.3) on increasing the temperature, following Arrhenius trend (Figure 2.9.).

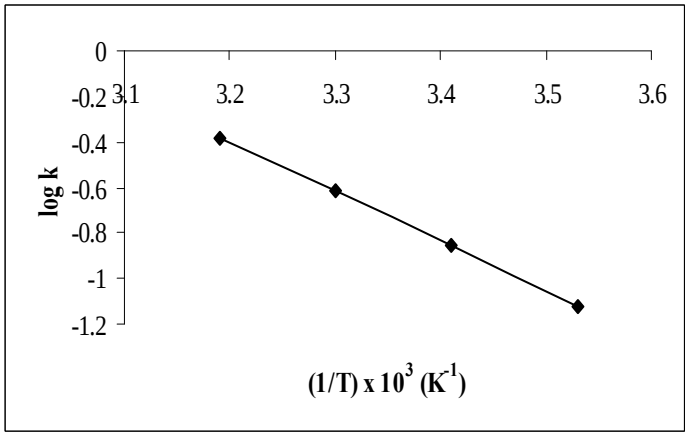

Figure 2.9. Plot of log k v/s 1/T (Arrhenius plot)

The value of activation parameters, E_a, $\Delta H^{\#}$ and $\Delta S^{\#}$ corresponding to the rate constants k given in Table 2.4. indicated that formation of complex **2** is associated with low energy of activation and highly negative entropy of activation favoring the rate of complexation

ition of CO with **1a**, in 1:1 (v/v) water-dioxan solvent. Complexation reaction indicated that the nature of complexation is associative. Almost identical $\Delta H^{\#}$ (39.7 kJ mol^{-1}) and comparable $\Delta S^{\#}$ (-107.0 JK^{-1} mol^{-1}) are reported [29] for carbonylation of Ru-EDTA system in aqueous medium in the studied temperature range 15-45^{0}C, suggesting that ruthenium complexes tend to have negative entropy of activation during complexation with carbon monoxide.

Formation constants K_1 were determined at different temperatures in the range 10-40^{0}C in order to see the effects of temperature on formation constant of complex **2** and to evaluate the thermodynamic parameters. The temperature-dependence formation constants and thermodynamic parameters are given in Tables 2.1. and 2.4. respectively. The formation constants (Table 2.1.) were decreased on increasing the temperature and were in agreement with vanâ Hoff equation. A plot of logK_1 versus 1/T (Figure 2.10.) was found to be almost linear.

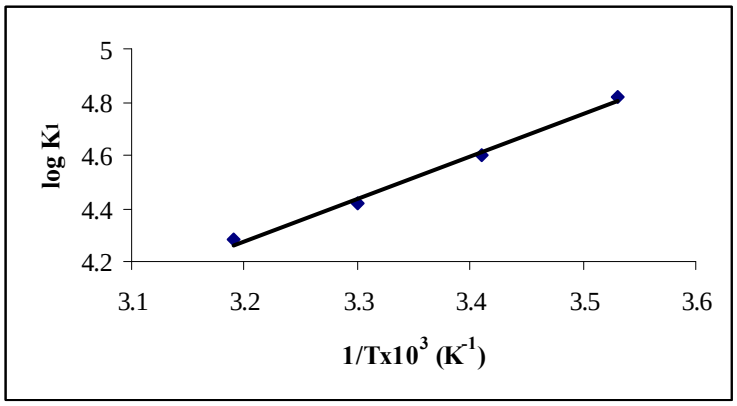

Figure 2.10. Plot of log K_1 v/s 1/T

All the thermodynamic parameters corresponding to the formation constant K_1 are associated with negative values. Highly negative value of enthalpy of formation ΔH^0, indicated that the formation of complex **2** is exothermic. The formation of complex **2** is thus favorable, associated with negative values of ΔH^0 and ΔG^0. Both entropy of activation and entropy of formation, of complex **2** were favorable being associated with highly negative values. Hence, both, activation as well as thermodynamic parameters were found to be favorable for the formation of complex **2**.

…opylene using $RuCl_2(PPh_3)_3$ as a catalyst

…e catalytic activity of $RuCl_2(PPh_3)_3$ for hydroformylation of propylene, a series of catalytic experiments were conducted at 9 bar pressure of carbon monoxide, hydrogen and propylene with 1:1:1 pressure ratio at 175^0C temperature in 50 ml solvent ethanol. The hydroformylation was examined at different catalyst concentrations in the range $2.5x10^{-3}$ to $10x10^{-3}$ mM and the results are given in Table 2.5. The conversions were found to be low; indicating that the catalyst is less active for hydroformylation, a comparison of catalyst concentration variation indicated that at concentration of $2.5x10^{-3}$ mM of catalyst, both conversion as well as selectivity was relatively better. Although, the low catalytic activity of ruthenium complexes for hydroformylation reactions are reported [30] earlier also, but the reasons for the low activity for hydroformylation are not well understood.

Table 2.5. Conversion and selectivity data for the propylene[a] hydroformylation with catalyst. **1**

Run	[Cat] (mM)	Conversion (%)	C_4-aldehydes (%)	C_4-alcohol (%)
1	2.5	37.86	10.49	5.91
2	5.0	30.08	9.81	15.07
3	7.5	33.32	5.05	5.03
4	10.0	33.57	6.98	13.39
5	2.5[b]	34.44	9.63	7.38
6	1.0[c]	38.28	-	-

[a]*Reaction conditions*: $p(CO+H_2)$ = 6 bar, $p(C_3H_6)$ = 3 bar, T = 175^0C, Solvent (Ethanol) = 50 ml, reaction time = 5h, [b]*Reaction conditions*: T = 120^0C, solvent (Chloroform) = 50 ml, [c]*Reaction conditions*: catalyst = isolated solid containing complex **3** and **4**, solvent (Dichloromethane) = 50 ml.

In our investigations, detailed studies were performed to understand the reason for the low activity of $RuCl_2(PPh_3)_3$, for the hydroformylation of propylene. It was observed that few crystals were precipitated out in the autoclave reactor during propylene hydroformylation reactions under employed reaction conditions. These crystals were analyzed by physicochemical methods as dicarbonyldichlorobis(triphenylphosphine)ruthenium(II), $RuCl_2(CO)_2(PPh_3)_2$, **3** and dicarbonylchlorohydridobis(triphenylphosphine)-ruthenium(II), $HRuCl(CO)_2(PPh_3)_2$, **4**. Single crystal X-ray structure of one of the

o determined to understand the isomerism present in oncluded that precipitation of the intermediate species **3** and **4** during hydroformylation reaction cycle was to be one of the reasons for the low activity of the complex **1** under employed reaction conditions.

2.3.5. Studies on isolated complexes formed during hydroformylation of propylene

The C, H and N analysis obtained for the separated solid mixture during hydroformylation reaction was as: C, 63.3; H, 4.3. The FT-IR spectra of the isolated mixture (Figure 2.11.) showed bands at 1881, 1999 and 2061 cm^{-1}. The IR band observed at ν = 1881 cm^{-1} [27, 31] confirms the presence of Ru-H bond. The ν(CO) bands at 2061 and 1999 cm^{-1} indicate the presence of two carbonyls coordinated to ruthenium center in *cis* configuration.

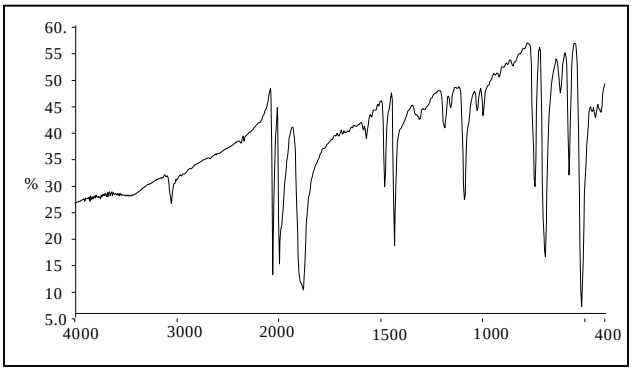

Figure 2.11. The IR spectra of solid mixture obtained during hydroformylation reaction

The ^{31}P NMR spectrum of the isolated solid gives two singlets at 34.81 and 72.75 ppm indicative of two non-equivalents phosphorous. If these two non-equivalents phosphorous are present in the same complex, one should get two doublets due to the presence of two non-equivalents phosphorous with P-P coupling. As ^{31}P NMR spectra gave only two singlets and it is obvious that these two ^{31}P singlets are originating from two different complexes. The ^{1}H NMR (Figure 2.12.) spectra of the isolated solid mixture gave one symmetrical triplets in the high field resonance at -4.5 ppm [*J(P-H)* = 19 Hz] in CH_2Cl_2, which implies the presence of a hydride *cis* to two equivalent phosphine [32].

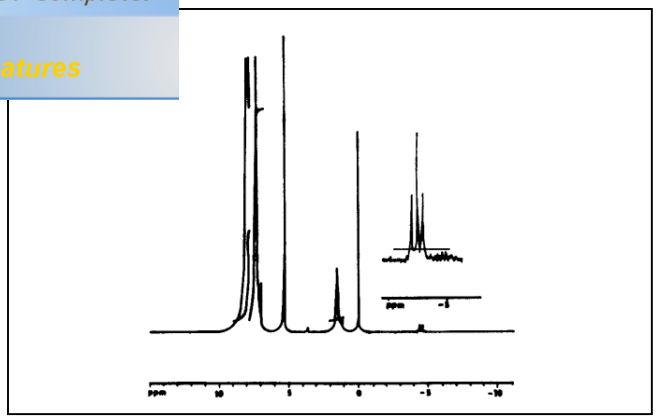

Figure 2.12. ^{1}H NMR of solid mixture obtained during hydroformylation reaction (insets: magnification of the triplets obtained at ï 4.5 ppm).

James et al. [33] have reported the interaction of H_2 and then CO to the coordinatively unsaturated 16-electron complex **1** in dimethylacetamide (dma), and isolated a mixture of complexes **3** and **4** as depicted in Scheme 2.1.

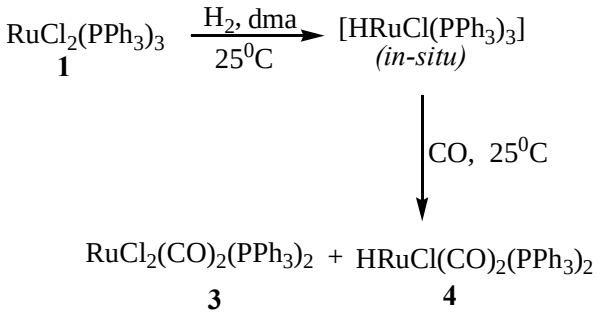

Scheme 2.1.

The symmetrical triplet structure of the high field hydride resonance in the ^{1}H NMR spectra implies that complex **4** may have one of the following isomeric structures.

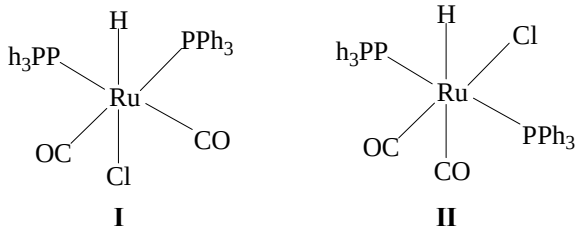

gand *trans* to hydride [34], makes isomer (II) more stable than isomer (I). In addition, the singlet obtained in ^{31}P NMR spectra at 72.75 ppm also confirms the *trans* position of phosphorous to each other {isomer (II)}.

c*is*-Ruthenium dicarbonyl complex **3** may exist in three isomeric forms; (III)ï (V). However, IR spectra of the isolated mixture gave ν(CO) [34] bands at 2061 and 1999 cm^{-1} and a ^{31}P NMR gave singlet at 34.81 ppm, thereby, inferring that *cis*-ruthenium dicarbonyl complex **3** may exist as isomer (III). The downfield shift of 38 ppm in ^{31}P chemical shift from the hydrido-ruthenium complex may be due to change in the electronic environment in the complex **3** because of the presence of *cis* carbonyls and chlorides groups.

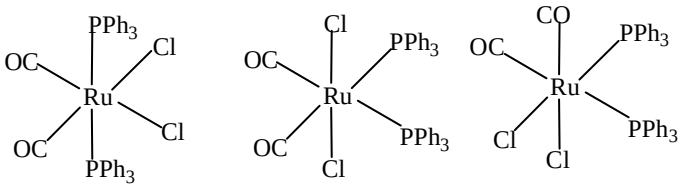

III **IV** **V**

The first sight of crystals obtained during hydroformylation reaction emerged to be a mixture of blackish hexagonal and light yellowish needle shaped crystals. It was found that only light yellowish needle shape crystals were suitable for single crystal X-ray diffraction studies. The single crystal X-ray analysis of complex **3** has already been established by Batista et al. [35]. A summary of crystallographic data and selected bond lengths and angles around the coordination sphere is given in *Annexure*. The structure (Figure 2.13.) and crystal data were exactly matching with the results obtained by Batista et al. [35].

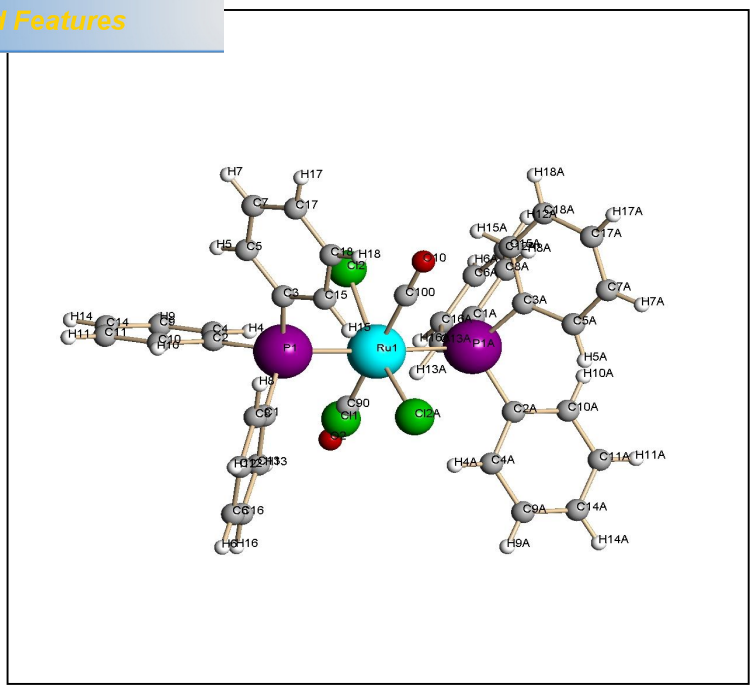

Figure 2.13. ORTEP diagram of complex **3** with atom numbering scheme (50% probability factor for the thermal ellipsoid).

2.3.6. Mechanism for the low activity of $RuCl_2(PPh_3)_3$ towards hydroformylation of propylene

The complexes **3** and **4** have been synthesized and studied by several researchers, however; it is for the first time that we are reporting the separation and characterization of complex **3** and **4** as intermediates under the hydroformylation reaction conditions, which, results the lower catalytic activity of complex **1** in hydroformylation of propylene. The formation and precipitation of intermediate complexes **3** and **4** during hydroformylation of propylene by complex **1** as a catalyst may be one of the reasons for its low activity towards hydroformylation under mild pressure conditions. In order to ensure the above-mentioned possibility, the catalytic inactivity of the isolated complexes **3** and **4**, hydroformylation of propylene catalyzed by isolated mixture was done using dichloromethane as a homogenous solvent for the complexes. Although, 38% conversion to isomerized/hydrogenated products was observed, but no hydroformylation activity was observed for these complexes as seen from the absence of C_4-aldehydes and C_4-alcohols in the product mixture (Table 2.5.). The $RuCl_2(PPh_3)_3$, **1**, catalyzed hydroformylation of

l in a solvent in which the complex **3** and **4** are soluble 5% conversion of propylene with 9.6% selectivity for C_4-aldehydes and 7.4% selectivity for C_4-alcohols. These conversion data are similar to those obtained in the solvent where complex **3** and **4** are insoluble and precipitate out (Table 2.5.). This confirms that formation of complex **3** and **4** is responsible for the low hydroformylation activity of $RuCl_2(PPh_3)_3$ catalyzed hydroformylation of propylene. The possible mechanism for the formation of inactive intermediates **3** and **4**, and thereby lower activity of complex **1** for hydroformylation of propylene (Table 2.5.) is discussed below.

The complex **1** may interact with propylene to give alkene complexes as have been reported [36] or it may interact with syn-gas to give the complex **3** and **4** as reported by James et al. [33]. These two possibilities strongly depend on the solubility of these gases in ethanol. The ethoxide-ruthenium complex from ethanol-ruthenium system as reported by Chatt et al. [31] is also one of the possibilities for the formation of ruthenium hydride complex. Although this reaction was base promoted, may be in our case, the hydroformylation reaction conditions can promote the formation of Ru-H complex.

Thus, during the hydroformylation of propylene, the complex **1** may have higher tendency to form insoluble complex **3** and **4** than complex **5** (Scheme 2.2.) which is an intermediate complex responsible for hydroformylation products. Here, in the first step (a) the interaction of hydrogen with coordinatively unsaturated 16-electron complex **1** gives the hydride complex **4a**. This complex **4a** has tendency to form either complex **3** and **4** through step (c) (Scheme 2.2.) or hydroformylation products through step (b) and (c′) via formation of complex **5**. The *cis*-dicarbonyl complex **3** and hydride complex **4** (*vide supra*) were being separated in alcoholic solution as a solid crystalline complexes during hydroformylation reaction showing preferred formation of these intermediates. Consequently, the interaction of propylene to complex **5** is very weak and hence lower conversions of hydroformylation products.

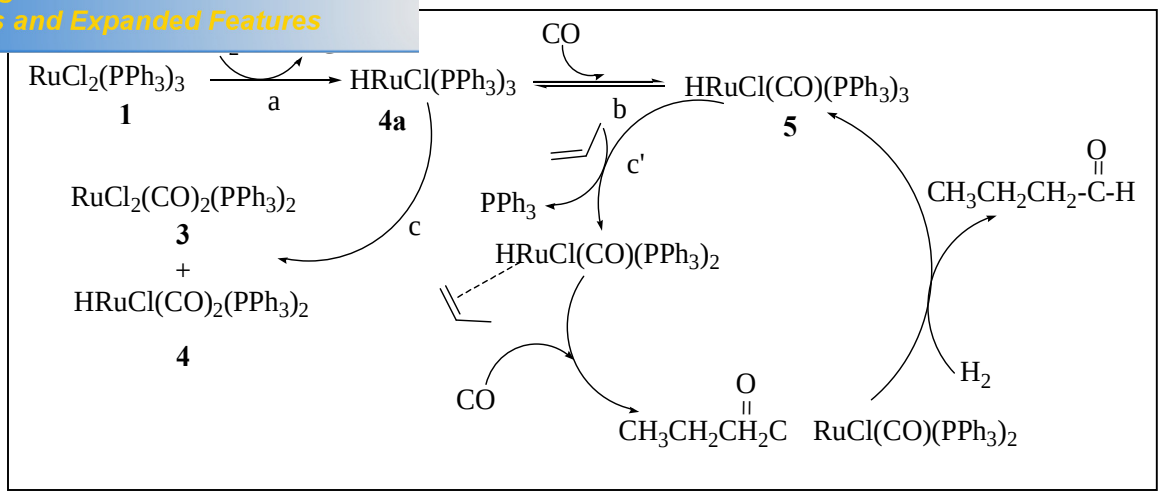

Scheme 2.2. The plausible mechanism of formation of complex **3** and **4** together with hydroformylation products.

armar, R.V. Jasra, *Chemical Weekly*, Part 1: Commercial Aspects, July 8 (2003) 173.

2. V.K. Srivastava, D.U. Parmar, R.V. Jasra, *Chemical Weekly*, Part 2: Technology, July 15 (2003) 181.
3. C.L. Aldridge, H.B. Jonassen, *J. Am. Chem. Soc.*, **85** (1963) 886.
4. J. March, *Advance Organic Chemistry*, IV Ed. Wiley-Interscience Publication p. 810.
5. R.A. Sanchez-Delgado, J.S. Bradely, G. Wilkinson, *J.C.S. Dalton Trans.*, (1976) 399.
6. G. Suss-fink, G.F. Schmidt, *J. Mol. Catal.*, **47** (1987) 361.
7. G. Suss-fink, G. Herrmann, *J. Chem. Soc., Chem. Commun.*, (1985) 735.
8. G. Suss-fink, *J. Organomet. Chem.*, **193** (1980) C20.
9. M.K. Makiewicz, M.C. Baird, *Inorg. Chim. Acta*, **113** (1986) 95.
10. F.J. Waller, *J. Mol. Catal.*, **31** (1985) 123.
11. M.M. Taquikhan, S.B. Halligudi, S.H.R. Abdi, *J. Mol. Catal.*, **44** (1988) 179.
12. M.M. Taquikhan, S.B. Halligudi, S.H.R. Abdi, *J. Mol. Catal.*, **45** (1988) 215.
13. M.M. Taquikhan, S.B. Halligudi, S. Shukla, *Angew. Chem. Int. Ed. Engl.*, **27** (1988) 1735.
14. D.D. Perrin, W.L.F. Armarego, D.D. Perrin, *Purification of Laboratory Chemicals*, 2nd ed., Pegamon Press, p. 249.
15. A.I. Vogal, *Textbook of Practical Organic Chemistry*, Orient Longmans, (1976).
16. T.A. Stephenson, G. Wilkinson, *J. Inorg. Nucl. Chem.*, **28** (1966) 945.
17. B.R. James, L.D. Markham, *Inorg. Chem.*, **13** (1974) 97.
18. V.K. Srivastava, S.D. Bhatt, R.S. Shukla, R.V. Jasra, *React. Kin. & Catal. Lett.*, **81** (2004) 99.
19. M.M. Taquikhan, R.S. Shukla, A. Prakash Rao, *Inorg. Chem.*, **28** (1989) 452.
20. L.K. Brown, *Inorg. Chim. Acta*, **37** (1979) 513.
21. M.M. Taquikhan, R.S. Shukla, *J. Mol. Catal.*, **71** (1992) 157.
22. CAD4-PC Software, Version 5, *Enraf-Nonius*, Delft, (1989).

I. P. Charland, F. L. Lee, P. S. J. White, *Appl. Cryst.*, **22**

24. G. M. Sheldrick, SHELX-*97*, *Program for Crystal Structure Determination*, Univ. of Göttingen, Germany, (1997).
25. B.R. James, L.D. Markham, B. C. Hui, G.L. Rampel, *J. Chem. Soc. Dalton Trans.*, (1973) 2247.
26. M.I. Bruce, F.G.A. Stone, *J. Chem. Soc. (A)*, (1967) 1238.
27. F. LõEplatteneir, F. Calderazzo, *Inorg. Chem.*, **7** (1968) 1290.
28. H. Stephen, and T. Stephen, *Solubility of Inorganic and Organic Compounds*, Pergamon Press, New York, (1963).
29. M.M. Taquikhan, A. Hussain, M.A. Moiz, R.M. Naik, *Polyhedron*, **8** (1989) 2199.
30. D. Evans, J.A. Osborn, F.H. Jardine, G. Wilkinson, *Nature*, **5016** (1965) 1203.
31. J. Chatt, B.L. Shaw, A.E. Field, *J. Chem. Soc. (A)*, (1964) 3466.
32. B.R. James, L.D. Markham, B.C. Hui, G.L. Rampel, *J.C.S. Dalton Trans.*, (1973) 2247.
33. B.R. James, L. D. Markham, *Inorg. Nucl. Chem. Lett.*, **7** (1971) 373.
34. H. D.F. Kaesz, R. B. Saillant, *Chem. Rev.*, **72** (1972) 231.
35. A.A. Batista, J. Zukerman-Schpector, O.M. Porcu, S.L. Queiroz & M.P. Araujo *Polyhedron*, **13** (1994) 689.
36. D.J. Cole-Hamilton, G. Wilkinson, *J.C.S. Chem. Commun.*, (1977) 57.